Local Run-Up Amplification by Resonant Wave Interactions

Themistoklis S. Stefanakis[1,2] and Frédéric Dias[2,1,*]

[1]*CMLA, ENS Cachan, 61 avenue du Président Wilson, 94235 Cachan cedex, France*
[2]*School of Mathematical Sciences, University College of Dublin, Dublin, Ireland*

Denys Dutykh[3]

[3]*Université de Savoie-CNRS Laboratoire de Mathématiques LAMA - UMR 5127 Campus Scientifique*
73376 Le Bourget-du-Lac, France

Until now, the analysis of long wave run-up on a plane beach has been focused on finding its maximum value, failing to capture the existence of resonant regimes. One-dimensional numerical simulations in the framework of the nonlinear shallow water equations are used to investigate the boundary value problem for plane and nontrivial beaches. Monochromatic waves, as well as virtual wave-gage recordings from real tsunami simulations, are used as forcing conditions to the boundary value problem. Resonant phenomena between the incident wavelength and the beach slope are found to occur, which result in enhanced run-up of nonleading waves. The evolution of energy reveals the existence of a quasiperiodic state for the case of sinusoidal waves. Dispersion is found to slightly reduce the value of maximum run-up but not to change the overall picture. Run-up amplification occurs for both leading elevation and depression waves.

Despite mathematical difficulties, wave run-up, which is the maximum vertical extent of wave uprush on a beach above still water level [1], has been extensively studied during the last 50 years. Progress was first made to the one-dimensional long wave problem. From the 1950s until 1990, several major contributions were made to the initial value problem of long wave run-up [2–6], mainly through the use of the Carrier and Greenspan [2] (CG) transformation, that allows the reduction of the two nonlinear shallow water equations (NSWEs) into a single linear equation. After the two 1992 tsunamis (Nicaragua and Flores Island), measurements suggested that the shoreline receded before inundation took place, an observation that lead Tadepalli and Synolakis [7] to propose a new *N*-shaped wave profile as a leading wave model. Recently, a more geophysically relevant *N*-wave model was derived, and the resulting run-up on a plane beach was computed [8]. Apart from the plane beach geometry, wave evolution and run-up have also been addressed for piecewise linear topographies [9]. Expressions for long wave run-up that are independent of the initial waveform were derived by Didenkulova and Pelinovsky [10]. All the above results dealt with the initial value problem. Antuono and Brocchini [11] solved the boundary value problem (BVP) for the NSWE, using the CG [2] transformation, and applied a perturbation approach by assuming small incoming waves at the seaward boundary. Later, the same authors [12] solved the BVP in physical space without use of the CG [2] transformation.

Concerning the two-dimensional problem, the sole analytical solution was derived by Brocchini and Peregrine [13] who used a transformation to relate the longshore coordinate to the time variable. This operation allowed them to use an expression for the horizontal velocity that reduced the dimensions and transformed their problem into the already solved one-dimensional canonical problem. However, their solution is only valid for mild angles of incidence.

Almost all of the aforementioned studies focus on the value of the maximum run-up. Nevertheless, extreme run-up values measured by field studies, like during the 17 July 2006 Java event [14], cannot be explained by the existing theory. Furthermore, in some cases, on the aftermath of a tsunami catastrophe, it has been reported that it was not the first tsunami wave that caused the maximum damage. In order to explain this phenomenon, scientists assume that the amplified maximum run-up values of nonleading tsunami waves are due to reflection and refraction effects from nearshore topographic features [15]. It is found that changes in bathymetry (i.e., underwater topography) may result in wave resonance [16–19]. In the present study, with the use of one-dimensional numerical simulations, we attempt to elucidate the run-up amplification by nonleading long waves.

The maximum wave run-up for the geometry of Fig. 1 was first studied for three different beach slopes, namely, $\tan\theta = 0.13$, 0.26, and 0.3, using incident monochromatic waves at $x = -L$ of the form $\eta(-L, t) = \pm\eta_0 \sin(\omega t)$, $\omega/\sqrt{g \tan\theta/L} \in (0, 6.29)$.

The maximum run-up for a given beach slope was found to depend on the incident wavelength (Fig. 2). For all three slopes, the maximum run-up is highest when the nondimensional wavelength $\lambda_0/L \approx 5.1$ (i.e., at $L = 100$ m offshore, the resonant wavelength is $\lambda_0 = 510$ m), where $\lambda_0 = 2\pi\sqrt{gL \tan\theta}/\omega$ is the wavelength of the incident
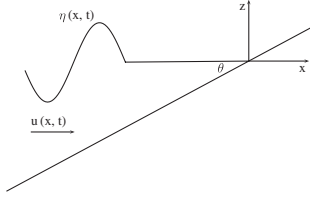
FIG. 1.   Geometry of the run-up problem.

wave. For increasing slope, the maximum run-up also increases and reaches an amplification factor $R_{\max}/\eta_0 = 59.76$ when $\tan\theta = 0.3$, which clearly is extremely high. Increasing the beach length leads to higher resonant maximum run-up values, as well as a secondary resonant regime at $\lambda_0/L = 1.5$. Amplification is seen for both leading elevation and depression waves. Adding dispersion to the system [20] only results in a reduction of the maximum run-up value at the resonant frequencies, without qualitatively changing the overall picture. The aforementioned values of maximum run-up were not achieved by the first incident wave, as is the case for $\lambda_0/L > 10$, but by subsequent ones (Fig. 3), thus signifying the existence of some resonant phenomena, the controlling parameters of which are the incident wavelength and the beach slope. Enhanced but not as extreme run-up is also present for wavelengths which are approximately half the resonant ones, an observation that strengthens the assumption that the harmonics play an important role on the run-up. The existence of resonant regimes is not predicted by linear theory [21], according to which $R_{\max}/\eta_0 = 2\pi\sqrt{2L/\lambda_0}$ (Fig. 2). However, the theory is in close agreement with the computed results in the absence of resonance.
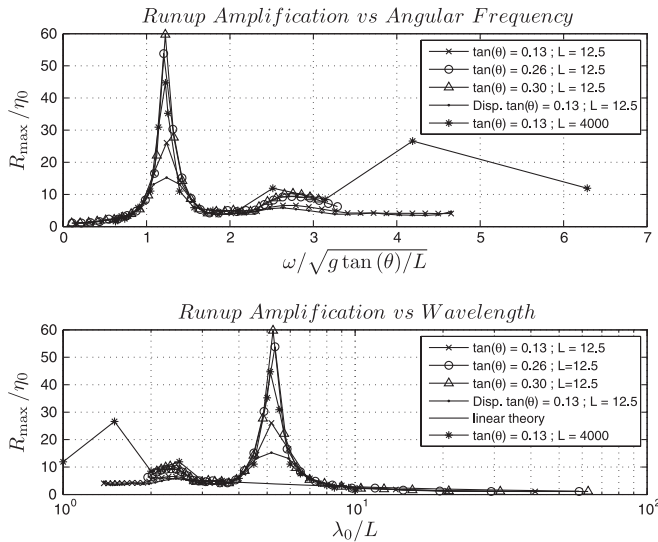
Figure 3 also shows that waves with both resonant and nonresonant frequencies reach a quasiperiodic state of equilibrium, which is reached faster when the frequency is nonresonant. A key difference is the existence of a single peak (trough) [run-up (run-down)] at the quasiperiodic state of the resonant regime, while the nonresonant frequencies show multiple peaks (troughs) in their quasiperiodic states. This is indicative of the importance of the synchronization between the incident and reflected waves on the run-up and run-down.

Next, we describe this novel resonant mechanism in terms of energy. The potential and kinetic energy of the wave are, respectively [22], $E_K = \frac{1}{2}\rho \int_{\mathbb{R}} \int_{-h}^{\eta} u^2 dx dz$ and $E_P = \frac{1}{2}\rho g \int_{\mathbb{R}} \eta^2 dx$. The kinetic energy can be reformulated in terms of the total flow depth $H = \eta + h$ as $E_K = \frac{1}{2}\rho \int_{\mathbb{R}} H u^2 dx$.

The evolution of the energy for the resonant frequency ($\omega = 0.4$ s^{-1}) when $\tan\theta = 0.13$ is shown in Fig. 4. One can see that both the maximum potential and kinetic energies increase with time until the quasiperiodic state is reached ($t\sqrt{g\tan\theta/L} \approx 30$). The potential energy takes its maximum value at the instance of the maximum run-up, when the kinetic energy is minimum. However, it is obvious that the maximum potential energy is approximately 5 times larger than the maximum kinetic energy. The impressive oscillations in the total energy are due to the large changes of the portion of the computational domain covered by water during run-up and run-down, which actually affects the limits of integration in the energy equations.

In Fig. 5, four different snapshots of the energy density distribution during run-up are shown in order to shed more light on the resonant mechanism ($\omega = 0.4$ s^{-1}, $\tan\theta = 0.13$). The first snapshot is taken at the instant

FIG. 2.   Maximum run-up amplification ratio as a function of nondimensional angular frequency (top) and nondimensional wavelength (bottom) for two beach lengths, namely $L = 12.5$ m and 4000 m.
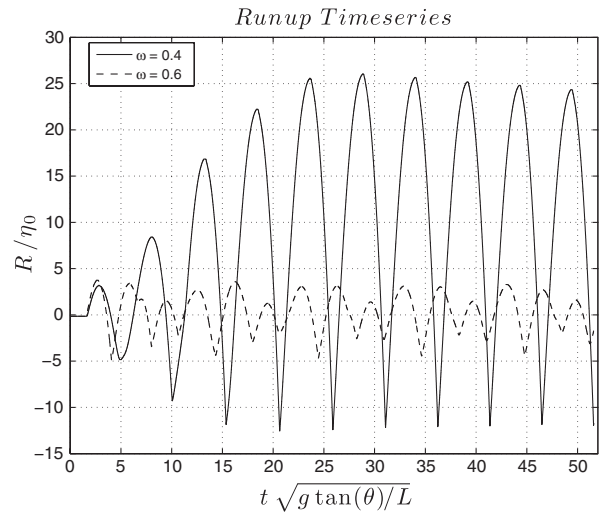
FIG. 3.   Run-up time series for two different angular frequencies: $\omega = 0.4$ s^{-1}, which is the resonant frequency for $\tan\theta = 0.13$, and $\omega = 0.6$ s^{-1}, which is a nonresonant frequency for the same slope ($L = 12.5$ m).
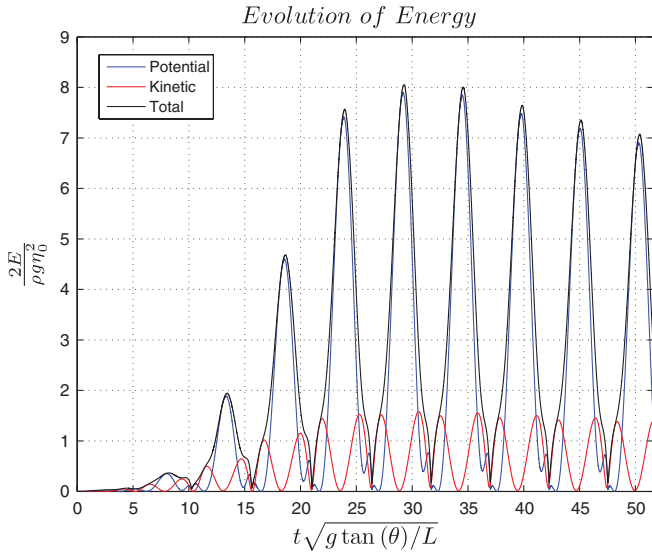
FIG. 4 (color).   Energy evolution time series for the resonant frequency $\omega = 0.4 \text{ s}^{-1}$ for $\tan\theta = 0.13$, $L = 12.5$ m.

when the first incident wave hits the initial shoreline. The potential energy is higher than the kinetic energy, and both of them are concentrated close to the shoreline. After the run-up of the first wave, the energy is reflected offshore, while at the same time energy is transferred shoreward

by the second incident wave, causing an amplification of kinetic energy. The same process is repeated by the following incident and reflected waves until the quasiperiodic state is reached. What is interesting is that the horizontal location where the amplification takes place remains almost stationary across run-ups and lies closer to the left boundary than the initial shoreline. After energy is amplified locally, it travels shoreward, possibly due to the continuous forcing at the left boundary.

Apart from idealistic simulations with sinusoidal waves, we explored whether similar resonant phenomena can occur during a real tsunami. Therefore, a simulation was run for the 25 October 2010 Mentawai Islands tsunami. A virtual wave gage was placed at Lon = 100.24° E, Lat = −3.4° N, where the depth is approximately 120 m, and the free surface elevation was obtained for the first 10 800 s of the tsunami [Fig. 6(a)]. From that data, only the first 2000 s were used as boundary value using a uniform slope $\tan\theta = 0.03$, which is close to the actual mean slope from the location of the wave gage to the closest shore (the distance of the wave gage to the shore is $L = 4000$ m). The time series of the shoreline elevation is shown in Fig. 6(b). We can observe the run-up of three waves at $t = 720$ s, $t = 1320$ s, and $t = 1860$ s. It is clear that the first wave does not cause the highest run-up, even though it has the highest amplitude, as recorded by the wave gage.
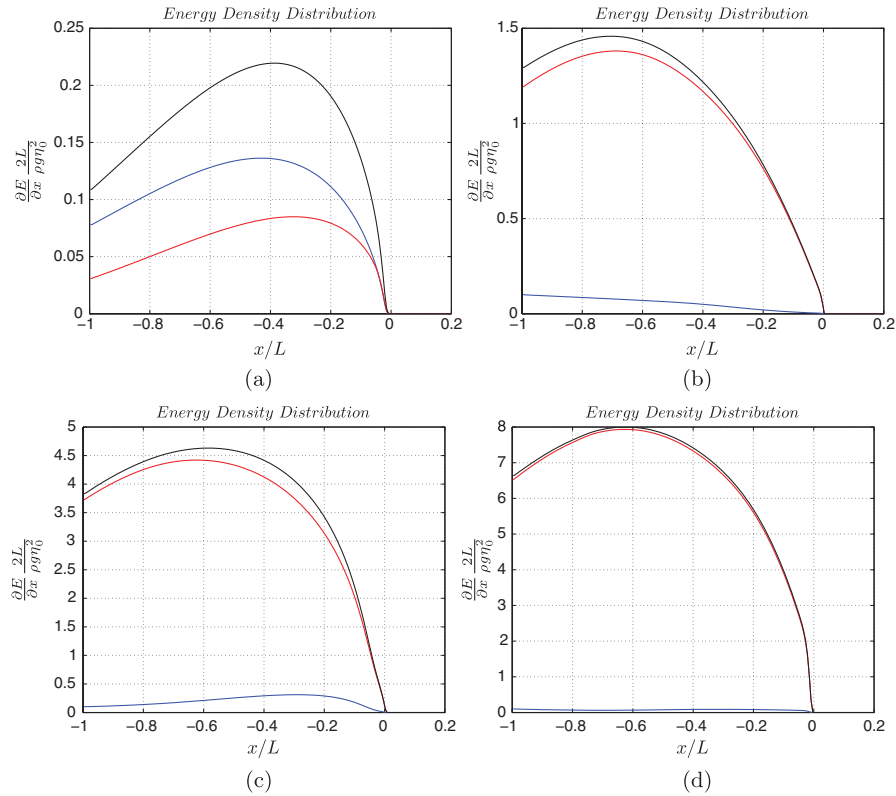
FIG. 5 (color).   Energy density distribution during run-up for the case of the resonant frequency ($\omega = 0.4 \text{ s}^{-1}$) when $\tan\theta = 0.13$ and $L = 12.5$ m, at the arrival of the (a) first, (b) second, (c) third, and (d) fourth waves. Note: the scale of the vertical axis differs between the four snapshots, and the color code is the same as in Fig. 4.
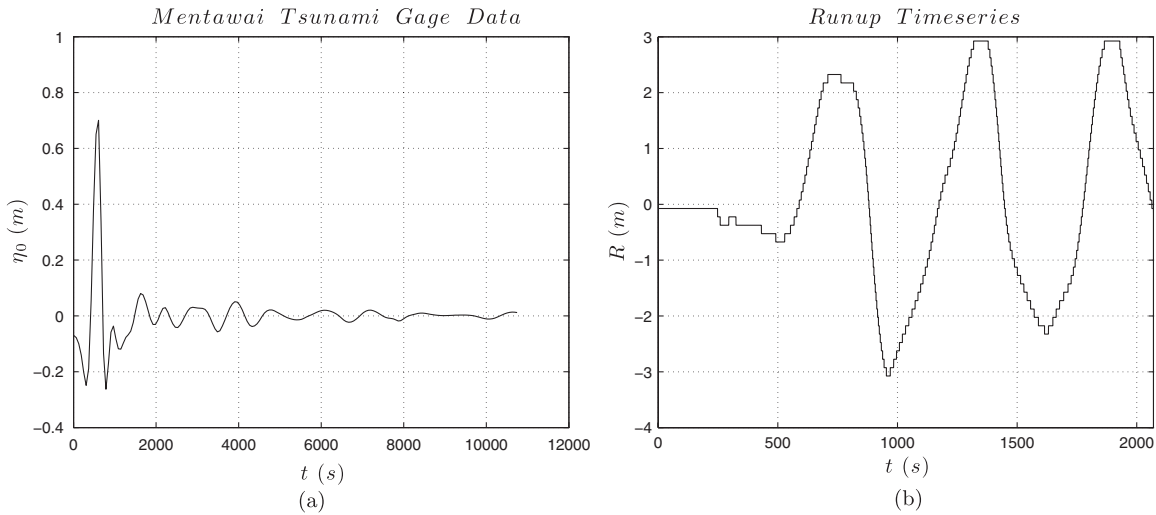
FIG. 6. (a) Virtual wave-gage (Lon $= 100.24°$ E, Lat $= -3.4°$ N) data obtained for the 25 October 2010 Mentawai Islands tsunami. (b) Time series of the shoreline elevation during the first 2000 s.

The fact that the highest run-up is not driven by the leading and highest wave excited our curiosity to investigate whether there exists a connection between the resonant mechanism observed when using sinusoidal wave profiles and the wave-gage recordings. From Fig. 6(b), one can see that the maximum run-ups are separated by

approximately 600 s intervals. If we assume that the incident wave is a sum of sinusoidal waves and $T = 600$ s is the period of the dominant mode, we can find the wavelength of that mode using $\lambda_0 = T\sqrt{gL\tan\theta}$. By doing so, the ratio λ_0/L is equal to 5.15 which, according to our previous results (Fig. 2), corresponds to the resonant
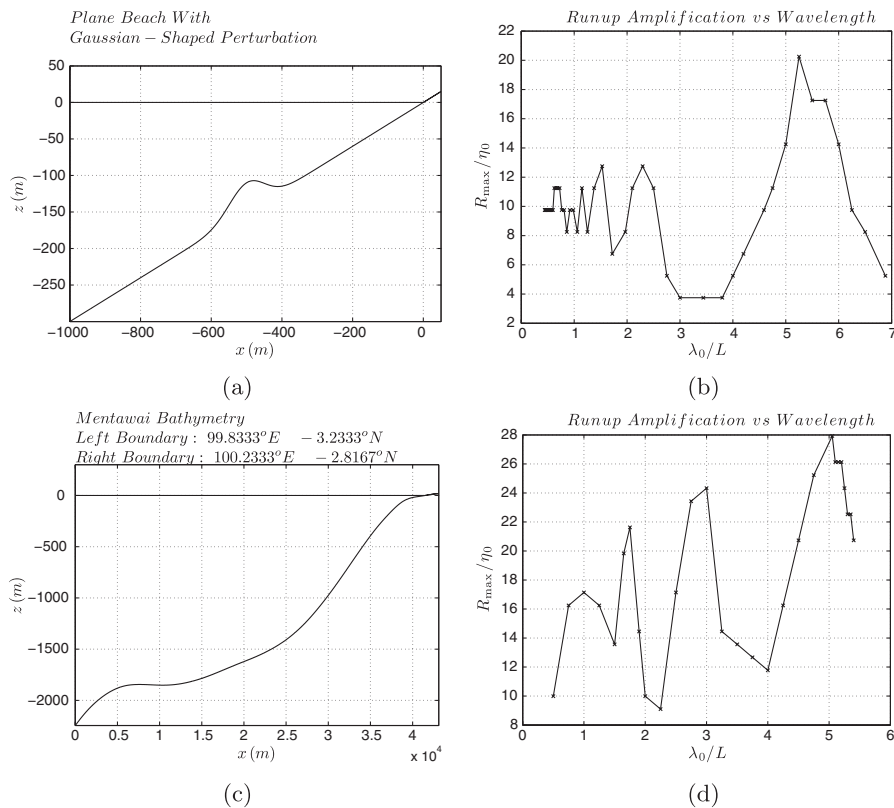
FIG. 7. (a) Plane beach perturbed by a Gaussian-shaped bathymetric feature. (b) Amplification ratio as a function of nondimensional wavelength. (c) Bathymetry in the Mentawai Islands region. (d) Amplification ratio as a function of nondimensional wavelength.

regime. Consequently, local resonant amplification of tsunami run-up may explain why in some cases it is not the first wave that results in the highest run-up.

In addition to simulations with a plane beach, we investigated two cases of nontrivial bathymetry. The first consists of a beach perturbed by a Gaussian-shaped underwater feature, as in Fig. 7(a). Again, the forcing at the boundary was an idealized sinusoidal signal, although this time it was limited to only four periods, since in nature one would not expect a wave train larger than that. In Fig. 7(b), we can observe the existence of resonant frequencies, although now the amplification is not as high. What is intriguing is the existence of multiple peaks, signifying that resonant phenomena might occur much more often than expected. We reached the same conclusion when we studied the second case, which had a real bathymetry taken from the region of the Mentawai Islands [Fig. 7(c)]. Multiple resonant frequencies can also be observed in this case [Fig. 7(d)], thus further strengthening the suggestion that resonant run-up amplification due to wave interactions is not a rare phenomenon.

In summary, we discovered local resonant amplification phenomena related to the one-dimensional BVP of the NSWE on a plane beach. The resonance occurs due to incoming and reflected wave interactions, and the actual amplification ratio depends on the beach slope. These phenomena can explain why it is not always the first wave that causes the highest run-up, as well as why the tail of a single wave may produce leading-order run-up values. Resonant mechanisms are not limited to the plane beach paradigm but can be observed in more complex bathymetries, as well, thus suggesting that local run-up amplification is not a rare event. However, when the bathymetry is nontrivial, it is not clear to what extent resonance is attributed to wave trapping and generation of harmonics.

*frederic.dias@ucd.ie

[1] R. Sorensen, *Basic Coastal Engineering* (Springer, New York, 1997).
[2] G. F. Carrier and H. P. Greenspan, J. Fluid Mech. **4**, 97 (1958).
[3] J. Keller and H. Keller, ONR Research Report Contract No. NONR-3828(00), 1964.
[4] G. F. Carrier, J. Fluid Mech. **24**, 641 (1966).
[5] C. Synolakis, Ph.D. thesis, California Institute of Technology, 1986.
[6] C. Synolakis, J. Fluid Mech. **185**, 523 (1987).
[7] S. Tadepalli and C. E. Synolakis, Proc. R. Soc. A **445**, 99 (1994).
[8] P. A. Madsen and H. A. Schaffer, J. Fluid Mech. **645**, 27 (2010).
[9] U. Kanoglu and C. Synolakis, J. Fluid Mech. **374**, 1 (1998).
[10] I. Didenkulova and E. Pelinovsky, Oceanology **48**, 1 (2008).
[11] M. Antuono and M. Brocchini, Stud. Appl. Math. **119**, 73 (2007).
[12] M. Antuono and M. Brocchini, J. Fluid Mech. **643**, 207 (2010).
[13] M. Brocchini and D. H. Peregrine, J. Fluid Mech. **317**, 241 (1996).
[14] H. M. Fritz, W. Kongko, A. Moore, B. McAdoo, J. Goff, C. Harbitz, B. Uslu, N. Kalligeris, D. Suteja, and K. Kalsum *et al.*, Geophys. Res. Lett. **34**, L12602 (2007).
[15] S. Neetu, I. Suresh, R. Shankar, B. Nagarajan, R. Sharma, S. Shenoi, A. Unnikrishnan, and D. Sundar, Nat. Hazards 1 (2011).
[16] J. W. Miles, J. Fluid Mech. **28**, 755 (1967).
[17] K. Kajiura, in *Waves on Water of Variable Depth*, edited by D. Provis and R. Radok, Lecture Notes in Physics Vol. 64 (Springer-Verlag, Berlin, 1977), p. 72.
[18] Y. Agnon and C. C. Mei, J. Fluid Mech. **195**, 201 (1988).
[19] G. L. Grataloup and C. C. Mei, Phys. Rev. E **68**, 026314 (2003).
[20] D. Dutykh, T. Katsaounis, and D. Mitsotakis, J. Comput. Phys. **230**, 3035 (2011).
[21] E. N. Pelinovsky and R. K. Mazova, Nat. Hazards **6**, 227 (1992).
[22] D. Dutykh and F. Dias, Proc. R. Soc. A **465**, 725 (2009).